

1 Flexural Behaviour of Precast Segmental Concrete Beams Internally Prestressed
2 with Unbonded CFRP Tendons under Four-point Loading

3 Tan D. Le¹, Thong M. Pham², Hong Hao³ and Yifei Hao⁴

4
5 **Abstract**

6 This study investigates the use of carbon fibre reinforced polymer (CFRP) tendons on precast
7 segmental beams (PSBs) to tackle the corrosion problems which are likely to occur at joint
8 locations of PSBs prestressed with steel tendons. Up to date, the use of CFRP tendons was
9 extensively documented for monolithic beams while their application on PSBs has not been
10 reported yet. Three precast segmental T-section beams including two beams with unbonded
11 CFRP and one with steel tendons were built and tested under four-point loads in this study.
12 The test results showed that CFRP tendons can be well used to replace the steel tendons on
13 PSBs. The beams with CFRP tendons demonstrated both high strength and high ductility as
14 compared to the beam with steel tendons. However, the stresses in the unbonded CFRP tendons
15 at ultimate loading conditions of the tested beams were low, ranging from only about 66% to
16 72% of the nominal breaking tensile strength. The type of joints i.e. dry and epoxied, greatly
17 affects the initial stiffness of the beams but has no effect on the opening of joints at ultimate
18 loading stage. Moreover, a comprehensive examination on four existing code equations to
19 predict the stress in the unbonded tendons showed that the four examined codes predicted well

¹PhD Scholar, Center for Infrastructural Monitoring and Protection, School of Civil and Mechanical Engineering, Curtin University, Kent Street, Bentley, WA 6102, Australia. Email: tan.le1@postgrad.curtin.edu.au

²Research Fellow, Center for Infrastructural Monitoring and Protection, School of Civil and Mechanical Engineering, Curtin University, Kent Street, Bentley, WA 6102, Australia, (corresponding author). Email: thong.pham@curtin.edu.au

³John Curtin Distinguished Professor, Center for Infrastructural Monitoring and Protection, School of Civil and Mechanical Engineering, Curtin University, Kent Street, Bentley, WA 6102, Australia, and School of Civil Engineering, Guangzhou University, Guangzhou 510006, China, (corresponding author). Email: hong.hao@curtin.edu.au

⁴Professor, Key Laboratory of Coast Civil and Structure Safety of Ministry of Education, Tianjin University, Tianjin, 300072, China. Email: hao.yifei@tju.edu.cn

20 the stress at the ultimate loading condition of the unbonded steel tendons, however, they
21 significantly under predicted those in the CFRP tendons. A modification in the strain reduction
22 coefficient used by ACI 440.4R for predicting the stress increment in unbonded CFRP tendons
23 of monolithic beams is therefore proposed for PSBs based on the experimental results.

24 **Keywords:** segmental concrete beams; fibre reinforced polymer (FRP) tendons; internal
25 unbonded tendons; posttensioning; shear-keyed joints.

26 1 Introduction

27 Since its first application for concrete bridges in 1950's, precast segmental prestressed concrete
28 girder bridges have gained rapid acceptance as they not only allow speeding up the construction
29 process but also improving the quality control. So far, steel tendons have been used as the only
30 prestressing solution to connect individual beam segments to form the completed bridge spans.
31 The steel tendons can be bonded or unbonded to the concrete and placed inside or outside of
32 the beam cross-section, known as internally or externally prestressing techniques. Corrosion of
33 steel tendons at joint locations, however, causes deterioration or even total collapse of the
34 whole structures [1-3] .

35 Fibre reinforced polymer (FRP) tendons have been used for the prestressing technique as a
36 promising solution to replace steel tendons to deal with the corrosion issue. The term "FRP
37 tendons" denotes the use of one of various types of fibres, i.e. aramid (AFRP), carbon (CFRP)
38 or glass (GFRP). In the literature, the use of FRP tendons have only been applied to monolithic
39 concrete beams [4]. When tendons are internally bonded to the concrete, FRP and steel
40 prestressed beams behave differently after concrete cracked [4-6]. In the first stage, both beams
41 with FRP and steel tendons will deform elastically until cracking of concrete. After cracking,
42 beams prestressed with steel tendons exhibits nonlinear load-deflection behaviour until the
43 beams fail by crushing of concrete or rupture of tendons. In contrast, beams prestressed with
44 FRP tendons will continue to deform in an approximately linear manner with the increase in
45 the applied load until the tendons rupture or the concrete reaches its ultimate compressive
46 strain. Furthermore, Maissen and de Smet [6] reported that the moment redistribution
47 mechanism in the beams prestressed with CFRP tendons differed from that of the beams with
48 steel tendons because CFRP tendons did not exhibit elasto-plastic deformation characteristics.
49 Zou [7] pointed out that the conventional ductility index for concrete beams prestressed with
50 steel tendons was not suitable for beams with FRP tendons since FRP did not have a yield

51 point. As such, a new deformability index counting for both deflection and strength factors was
52 proposed and it applied to beams with either FRP tendons or steel tendons. It is noted that this
53 proposed deformability index was based on the analysis of monolithic beams prestressed with
54 carbon fibre reinforced polymer (CFRP) tendons or steel tendons.

55 In cases of unbonded tendons, on the other hand, beams with FRP and steel tendons behave
56 very similarly [8-10]. The only difference is FRP tendons showed linear behaviour up to the
57 ultimate load and have lower elastic modulus as compared to steel tendons. Pisani [10]
58 numerically analysed simply supported beams prestressed with unbonded GFRP or steel
59 tendons and stated that the beams with unbonded GFRP tendons showed non-linear load-
60 deflection behaviour up to ultimate load, which was very similar to that of the unbonded steel
61 tendons beams. The ductility of the GFRP beams was even better, although their ultimate
62 strength was lower than beams reinforced with steel tendons. Similar observations were also
63 reported by Lou et al. [8] for beams externally prestressed with FRP tendons. Tan and Tjandra
64 [9] tested continuous beams and concluded that the use of external CFRP tendons did not lead
65 to significant differences in the ultimate loads, tendon stresses, and deflections as compared to
66 conventional steel tendons.

67 When FRP tendons are used for prestressing, stress concentration in the tendon due to harping
68 effect is an important factor that needs due care. The localized curvature generated by the
69 deviation will cause a high stress concentration in the tendons which adversely prevents the
70 tendons to fully achieve its breaking capacity. The effects of the deviator curvature, harped
71 angle, and tendon size are found to be the main factors impacting the stress increment in the
72 CFRP tendons accounting for the harping effect [11-14]. Mutsuyoshi and Machida [11] found
73 that CFRP tendons deviated at an angle of 11.3° ruptured at approximately 80% of their
74 breaking load when 400-mm diameter steel deviators were used. Grace and Abdel-Sayed [12]
75 reported 19% and 34% reductions in breaking forces for carbon fiber composite cable (CFCC)

76 tendons draped at 3° angle and 5° angles when using 50.8 mm diameter deviators. When 508
77 mm diameter deviators were used, those reductions were 12% and 26% at draping angles of 5°
78 and 10°, respectively. Quayle [13] found reductions ranging between 13% and 50% in the
79 tensile strength of the CFRP tendons when the tendons were draped at 2° to 15° with 50 mm to
80 1000 mm radii deviators, respectively. Based on finite element analysis on Basalt FRP tendons,
81 Wang et al. [14] recommended a bending angle less than 3° to avoid the strength reduction
82 percentage exceeding 10%.

83 Joints between segments are the most critical part of PSBs as they permit the shear transfer and
84 integrity of the whole structure. The joints can be epoxied or dry, flat or keyed, and having
85 single or multiple shear keys and are made of plain concrete or reinforced concrete. The
86 behavior of joints under direct shear were extensively studied in the literature [15-17]. From
87 experimental tests on panels, Turmo et al. [17] concluded that the use of steel fibre reinforced
88 concrete (SFRC) did not increase the shear capacity of the panel joints. In addition, the
89 formulation recommended by AASHTO [18] yielded the best prediction for the shear capacity
90 of the joints as concluded by the authors.

91 This different feature between a segmental and a monolithic beam may cause further concern
92 to the PSBs as the opening of joint and sliding of segments may cause stress concentration in
93 the tendon and change the loading distributions in the beam. This, in turn, raises up a question,
94 is FRP tendon a good solution for prestressing PSBs despite owning excellent mechanical
95 properties? In other words, can the FRP tendon fully achieve its breaking capacity or will it
96 suffer from premature failure due to stress concentration at joint locations? Since FRP tendon
97 is made of an anisotropic material, it has very low transverse modulus and strength as compared
98 to those in the longitudinal direction.

99 This study, therefore, focuses on investigating the behaviour of PSBs prestressed with

100 unbonded CFRP tendons. As far as the authors are aware, this is the first time CFRP tendons
101 are applied to post tensioning segmental concrete beams. The effect of tendon types and joint
102 types on the structural behaviour of segmental concrete beams will be discussed.

103 **2 Experimental program**

104 To evaluate the use of CFRP tendons on PSBs, three large scale segmental concrete beams
105 including two beams post-tensioned with CFRP tendons and one beam with unbonded steel
106 tendons which served as a reference specimen were built and tested in the Civil Engineering
107 Laboratory, Curtin University. Two types of dry or epoxied multiple shear-keyed joints were
108 used in the beams. All the beams were then tested under four-point loading test up to failure.
109 The details of specimen design and test set up are described in the subsequent sections.

110 **2.1 Design of specimens**

111 All the specimens were made of reinforced concrete and were designed according to the
112 requirements of AASHTO [18] for segmental concrete beams and ACI 440.4R [4] for beams
113 prestressed with FRP tendons. The total length of a beam is 3.9 m with T-shape cross-section
114 of 400 mm height. Each beam consisted of four individual segments which were connected
115 together by two steel or CFRP tendons using the posttensioning technique. For convenience,
116 each specimen was labelled as given in Table 1, in which Beam BS1 was prestressed with two
117 steel tendons and had dry joints while Beams BC1 and BC2 was prestressed with CFRP tendons
118 with different joint types, i.e., dry or epoxied. Fig. 1 shows the design details and dimensions
119 of the tested beams.

120 Previous studies showed that the shear stress distribution in the multiple shear-keyed joints,
121 which are widely used in practice, is more uniform than in the single keyed joints [15, 16, 19].
122 As such, multiple shear-keyed joints were adopted in the present study. These shear keys had
123 the same cross-section size but different lengths on the flange and on the web of the specimens

124 as shown in Fig. 2.

125 Each segment of the beams was reinforced with the minimum amount of non-prestressed
126 reinforcement at the top and bottom of the segment. This minimum amount reinforcement was
127 in accordance with the requirements of ACI 318-14 [20] for beams with unbonded tendons.
128 The minimum area of the longitudinal reinforcement was computed as: $A_{s,min} = 0.004A_{ct}$, where
129 A_{ct} is the area of that part of the cross-section between the flexural tension face and the centroid
130 of the gross section. Two 12 mm diameter deformed bars were used for the bottom longitudinal
131 reinforcement and **four** 10 mm diameter deformed bars were used for the top layer. These steel
132 bars were cut off leading to the discontinuity of the longitudinal steel reinforcement at each
133 joint location. 10 mm diameter deformed bars were also used for transverse reinforcements
134 which were placed at 100 mm spacing for the two middle segments and at 75 mm spacing for
135 the two end segments to strengthen beams in shear (Fig. 1).

136 All the beams were under-reinforced according to strength design [18]. Beam BS1 has an
137 unbonded prestressing reinforcement ratio of $0.112\rho_b$, while those of **Beams** BC1 and BC2 are
138 $0.53\rho_b$ and $0.58\rho_b$, respectively. It is noted that ρ_b is the balanced prestressing reinforcement
139 ratio for an counterpart beam with bonded tendons, which was given by ACI 440.4R [4] and
140 presented in Eq. 1:

141
$$\rho_b = 0.85\beta_1 \frac{f'_c}{f_{pu}} \frac{\varepsilon_{cu}}{\varepsilon_{cu} + \varepsilon_{pu} - \varepsilon_{pe}} \quad (1)$$

142 where f'_c is the compressive concrete strength, ε_{cu} is the ultimate compressive strain of concrete
143 and taken as 0.003, f_{pu} and ε_{pu} are the design ultimate tensile strength and the corresponding
144 strain of CFRP tendon, respectively, and ε_{pe} is the effective strain in the CFRP tendon caused
145 by initial effective stress f_{pe} . It is noted that f_{pu} and ε_{pu} are replaced by the yield strength and the
146 corresponding strain of steel tendons when calculating the balanced reinforcement ratio for

147 Beam BS1.

148 **2.2 Materials**

149 Pre-mixed concrete was used in this experiment and was supplied by a local supplier.
150 Determination of concrete properties was conducted according to the Australian Standards AS
151 1012.8.1 [21] and AS 1012.9 [22] for concrete cylinders. The cylinders were of 100 mm
152 diameter and 200 mm height. The average compressive strength of three concrete cylinders on
153 the testing day was 44 MPa with a standard deviation of 1.47. Conventional steel bars of 12-
154 mm and 10-mm diameters were used for longitudinal and transverse steel reinforcements,
155 respectively. The ultimate tensile strength of 12-mm deformed bars N12 and 10-mm deformed
156 bars N10 were 587 MPa and 538 MPa, respectively, as provided by the manufacturer. 7-wire
157 12.7-mm diameter steel tendons and single strand 12.9-mm diameter CFRP tendons were used
158 in the specimens. The CFRP tendons were supplied by Dextra Building Products (GuangDong)
159 CO., LTD [23]. The mechanical properties of the CFRP tendons were reported by the
160 manufacturer after testing 16 CFRP coupons. Detailed properties of the materials used in the
161 specimens were given in Table 2.

162 **2.3 Casting of specimens**

163 Steel cages of each segment of all beams were prepared and placed in a timber formwork.
164 Corrugated metal duct of 40-mm diameter which was cut in designed length was also installed
165 into the steel cages to create holes for placing tendons later. To separate each segment during
166 pouring concrete, T-shape timber plates having the same dimension as beam's cross-section
167 were cut and placed in the formwork at intended locations as separation plates. Foam blocks
168 were attached to the separation plates to form the shear keys as shown in Fig. 3.

169 All segments were cast using match-casting method, i.e. the first and third segments were cast
170 in the first concrete batch, and then they were used as a formwork in the second batch to make

171 the second and fourth segments. By this way, it ensured the male and female keys perfectly fit
172 between two adjacent segments. Cylinders (100 mm diameter and 200 mm height) were also
173 cast to determine the concrete properties.

174 After casting, all the segments were cured in a moist condition in which wet hessian rags were
175 placed on top of the segments and were watered twice a day to keep them moist. The formwork
176 was removed after 7 days of casting, then the segments were left for continuous curing at least
177 28 days before post-tensioning and testing. Fig. 3 shows a typical segment at completion.

178 **2.4 Post-tensioning and epoxy**

179 Fig. 4 shows a photo of typical set up of post-tensioning. One end of CFRP tendons was
180 connected to a steel tendon via steel couplers as shown in Fig. 5. By this way, the prestressing
181 procedure for the CFRP tendons was done similarly to the steel tendons. It is noted that this
182 anchor design was made to ensure the tendon failure not to occur at the anchor region which
183 was therefore not a concern of this study. The stressing force was generated by a monostrand
184 hydraulic jack of 30 tons that seated onto a jacking chair. Two sets of wedges and barrel anchors
185 were used in the stressing end, in which one was placed after the hydraulic jack called post-
186 tensioning anchor #2 and another one was placed before the jack called working anchor #1.
187 Hollow bolts and nuts (tightening system) were placed inside the jacking chair just before the
188 working anchor for tightening and releasing the force later. 20-ton capacity load cells were
189 used to measure the tensioning force generated by the hydraulic jack and the force in the tendon
190 during the test.

191 For Beam BC2 with epoxied joints, the concrete surfaces of the shear keys were thoroughly
192 cleaned using a steel brush and an air gun to make sure the surface in a good condition and free
193 from dust. The concrete surfaces were then thoroughly watered and left to dry for at least 2
194 hours before applying the adhesive. A thin layer of Sikadur-30 [24] was applied to the joint

195 surfaces of the segments using a trowel. After posttensioning, the epoxied beam was left for
196 curing of the adhesive for 3 days.

197 The stressing procedure was done as follows. In the first step, the tendons were stressed an
198 initial force of approximately 10% of the total stressing force, F_s , to close the gaps between
199 segments and to remove the slack. F_s was computed from the control stress in the tendons,
200 which were taken as $0.75 f_{pu}$ for steel tendons [18] and $0.4 f_{pu}$ for CFRP tendons [4]. Then each
201 tendon was stressed in three load levels at 20%, 60% and 100% of the total stressing force until
202 completion. Load cells and strain gauges attached to the tendons were used to monitor and
203 measure the stresses in the tendons during the post-tensioning process. The effective tendon
204 stresses and the corresponding force in the tendons immediately following transfer are listed in
205 Table 1.

206 **2.5 Measurements, test set up and loading**

207 Measurements recorded during the tests include the applied load, vertical displacement,
208 opening of joints, strain in prestressing tendons and non-prestressing rebars. The applied load
209 was monitored by load cells attached to the hydraulic jacks. The load cells were calibrated to
210 have less than 1% error at the maximum loading capacity of 40 tons, and the error was smaller
211 at lower range, usually 0.5% to 1%. Linear variable differential transformers (LVDTs) of 100
212 mm measurement range were used for tracking the vertical displacement and opening of joints.
213 The accuracy of the LVDTs was around 0.5% to 1% over 100 mm span. Strain in the rebars
214 and prestressing tendons were measured by strain gauges and load cells attached at the end of
215 the beams as shown in Fig. 6. FLA-2 series of strain gauges supplied by Bestech Company [25]
216 were used in the tests.

217 The applied load was exerted by two vertical hydraulic jacks of 55 tons each placed equally at
218 one-third span. Two horizontal I steel beams were used to uniformly transfer the vertical loads

219 from the jacks to the beams. All the beams were tested under monotonic loads progressively
220 up to failure and the progressive loading pattern is shown in Fig. 7. Two load cycles were
221 performed at each loading level. The load increment in each loading level was 20 kN. In each
222 cycle, the applied load was gradually increased to the designated value of that loading level
223 and then was reduced to around 5 kN before starting the next cycles, except the first loading
224 cycle when the applied load started from 0. All the tests were carried out under load control at
225 a rate of 3 to 5 kN/min.

226 **3 Experimental results**

227 **3.1 Failure modes**

228 The tested results of all the specimens are shown in Table 3 in which P_y , P_u , $\delta_{mid,y}$, $\delta_{mid,u}$, $\Delta_{J,y}$,
229 $\Delta_{J,u}$ are the applied loads, midspan deflections, and openings of the middle joint of the
230 specimens at yielding and at ultimate condition, respectively. The definition of yielding point
231 is given in Section 3.3.

232 The failure of all the tested beams is shown in Fig. 8. The failure started by concrete crushing
233 on the top fibre followed by yielding of the steel tendons for Beam BS1 or rupturing of CFRP
234 tendons for beams prestressed with CFRP tendons. The crushing of concrete and rupture of
235 tendons occurred at the middle joint located at the midspan for all the beams. All the beams in
236 this study were under-reinforced in regards to a counterpart beam with bonded tendons,
237 therefore the failure mode would theoretically be tension controlled since $c/d < 0.42$ by
238 AASHTO LRFD [26] or $c/d < 0.375$ by ACI 318-14 [20], where c is the depth of the neutral
239 axis, d is the distance from the extreme top fibre to the centroid of tension force. However, the
240 test results show concrete crushing failure. In fact, unbonded tendons shifted the failure mode
241 of the under-reinforced counterparts from tension controlled to compression controlled. This
242 phenomenon may be attributed to the fact that the strain in the unbonded tendons does not

243 depend on the section analysis but the whole beam behaviour [27], which allows the beam to
244 achieve larger deflection leading to the higher compression strain in the concrete on the top
245 fibre. As a result, the calculation of the balanced reinforcement ratio for beams with **unbonded**
246 **tendons** requires further consideration. Lee et al. [28] found that the balanced reinforcement
247 ratio of a beam with unbonded tendons (ρ_b^U) was always smaller than that of a beam with
248 **bonded tendons** (ρ_b^B) and the ratio of ρ_b^U / ρ_b^B varied in a range between 0.43 and 0.83 for
249 specimens considered in their study.

250 **3.2 Load-deflection curves**

251 The load-deflection curves for all the specimens under four-point loading at different loading
252 levels are shown in Fig. 9. The envelop curves of these relations are plotted in Fig. 10. As
253 shown, Beam BC1 with unbonded CFRP tendons behaved very similar to Beam BS1 with steel
254 tendons. In both cases, the load-deflection curves were divided into two stages by a transition
255 zone. In the first stage, both beams had high stiffness and showed a linear relationship between
256 the applied load and deflection. In the second stage, the beams' stiffness sharply reduced and
257 the beams deformed in a non-linear manner up to failure. The transition from the first stage to
258 the second stage is related to the opening of the middle joint J2 under the applied loads. As
259 observed in Fig. 13, the middle joint J2 in Beams BS1 and BC1 **started to open** at the applied
260 loads of approximately 43.3 kN and 40.1 kN, respectively. At the same time, the stiffness of
261 the beams started to reduce dramatically. The only difference between the two beams **was** that
262 Beam BS1 had a higher initial stiffness than Beam BC1. However, after cracking Beam BS1
263 showed a lower tangent stiffness because of its lower reinforcement index, $\omega_{ps} = \frac{f_c'}{f_{pu}} \rho_{ps}$ where
264 ρ_{ps} is the reinforcement ratio. This behaviour is similar to segmental beams prestressed with
265 external steel tendons reported in previous studies [16, 29].

266 Similarly, the load-deflection curve of Beam BC2 with epoxied joints also exhibited two stages.
267 However, in the second stage, the beam still deformed almost linearly with the applied load up
268 to failure by rupture of the tendons. It is worth noting that the transition zone in the curve is the
269 result of concrete cracking in tension at bottom fibre at a load of approximately 44.7 kN. The
270 tensile crack was formed by one vertical crack cutting off all the shear-key bases of joint J2
271 located at midspan of the beam when the tensile stress generated by the applied load exceeded
272 the tensile strength of the concrete (Fig. 8c). Further details on this type of cracking are
273 discussed in the next section.

274 Type of joints also affected on the initial stiffness of the beams. As shown in Fig. 10, Beam
275 BC1 with dry joints had a lower initial stiffness as compared to Beam BC2 with epoxied joints.
276 This difference was resulted from the distinguished moment of inertia of the two beams in
277 which Beam BC1 with dry joint had the moment of inertia much smaller than that of Beam
278 BC2 associated with epoxied joints.

279 Previous studies [30, 31] showed that the response of monolithic beams with completely
280 unbonded tendons (without any ordinary tension reinforcement) is quite different from that of
281 beams with additional ordinary tension reinforcement as it behaves as a shallow tied arch after
282 cracking rather than a flexural member. Beam BS1 in this study may be considered as a beam
283 without any tension reinforcement as all the tension reinforcements were discontinued at joint
284 locations, however, the load-deflection curve had a good performance as it showed an
285 ascending branch after cracking. This is an additional benefit of segmental beams as compared
286 to monolithic ones associated with internal unbonded tendons.

287 **3.3 Ductility**

288 It is seen in Fig. 9 and Fig. 10 that all the specimens achieved large deflection before complete
289 failure. The maximum midspan displacement of Beam BS1 reached 89.4 mm which was equal

290 to 1/40 of the span length, L_b . The maximum midspan displacements of Beams BC1 and BC2
291 were 94.7 and 101.1 mm, corresponding to 1/38 and 1/35 L_b , respectively. It is noted that the
292 maximum allowable midspan displacement of these beams is $L_b/800$ according to AASHTO
293 LRFD [26]. These deflection capacities ensure to give engineers warnings before failure or
294 total collapse of the structures.

295 To reflect the physical behaviour of the tested beams in terms of ductility indices, two
296 calculation methods for the ductility of the beams, namely displacement ductility and energy

297 ductility were adopted in this study: Method 1, $\mu = \frac{\Delta_u}{\Delta_y}$ and Method 2, $\mu = \frac{A_u}{A_y}$, where Δ_u is

298 the ultimate midspan deflection; Δ_y is the midspan deflection of the beam at yielding of tension
299 steel; A_u is the area under the load-deflection curve at ultimate deflection, and A_y is the area
300 under the load-deflection curve at yielding of steel. The definition of yield point proposed by
301 Park [32] was adopted in this study and was illustrated in Fig. 11. The yielding of the structure
302 was due to the joint opening in cases of beams BS1 and BC1 and the concrete cracking in the
303 tension zone at beam's soffit in the case of Beam BC2. The ductility of the beams is presented
304 in Table 4.

305 It is seen from Table 4 that both the displacement ductility and energy ductility of Beam BS1
306 are higher than those of Beam BC1 although Beam BC1 achieved the maximum displacement
307 at 94.7 mm which was even larger than that of Beam BS1. The ductility of Beam BC2 is
308 approximately 3 times higher than that of Beam BS1. It can be noted that both the beams with
309 CFRP tendons have higher displacement capacity, and the ductility is governed by the yielding
310 displacement. This observation has proven that CFRP tendons can be used to replace steel
311 tendons to achieve the required strength and possibly even better ductility for segmental beams.
312 Interestingly, Beam BC2 had a ductility approximately 4 times higher than that of Beam BC1

313 as given in Table 4. However, it can be observed from Fig. 10, Beam BC1 showed similar
314 strength and deflection capacities as beam BC2. The reason for this big difference is due to the
315 variation in the value of the equivalent displacement at the yielding point. As shown, Beams
316 BC1 and BC2 had relatively similar maximum displacements and strengths but their yielding
317 points were different leading to the 4 times difference in ductility. It means that the ductility of
318 these beams is significantly governed by the displacement at the yielding point which can only
319 be approximately obtained from the testing data. The definition and calculation of ductility of
320 PSB beams prestressed with CFRP tendons with dry or epoxied joints need further verification.

321 **4 Discussions**

322 **4.1 Joint openings**

323 Fig. 12 shows the opening of all joints along beam's axis at the ultimate state. It can be seen
324 from the curves that in all the beams only the middle joints (J2) opened while the other joints
325 (J1 and J3) almost remained closed under the ultimate loads and the magnitude of the opening
326 at the ultimate load was nearly equal regardless of the types of joint used. This observation
327 confirms the assumption that the beam develops one major crack at the midspan at the ultimate
328 stage, which can be used to calculate the plastic hinge length and the stress in the unbonded
329 tendons in several models [33-35]. **These models assumed that the tendon elongation occurred**
330 **only at the opening hinge at the midspan of the beam.** The opening of the middle joint at the
331 ultimate state for Beams BS1, BC1 and BC2 was 30.44 mm, 27.70 mm and 30.02 mm,
332 respectively.

333 The opening of the middle joint J2 with respects to the applied loads for all the beams was
334 plotted in Fig. 13. It can be seen from the figure that the shapes of the applied load-joint opening
335 curves are very similar to the curves of the applied load and deflection for all the beams as
336 shown in Fig. 10. At the beginning, the joint still remained closed by the time it reached the

337 opening load or cracking load as discussed previously. After that, the joint started to open at a
338 much larger rate leading to the sudden reduction in the stiffness of the beams.

339 It is worth mentioning that the opening of joint J2 in Beam BC2, in fact, was the development
340 of a flexural vertical crack cutting off all shear-keyed bases as shown in Fig. 8c. The flexural
341 crack started from the bottom and quickly propagated to a certain height of the joint. This
342 phenomenon is because the tensile strength of the adhesive was much higher than the tensile
343 strength of concrete (20 MPa vs ~4 MPa) and there was no ordinary steel rebars through the
344 joint. After cracking, the middle joint in the epoxied beam behaved similarly to those in dry
345 joint specimens as seen in Fig. 12. It is noted that all joints completely closed when the load
346 was released at the end of each load level as the effect of prestressing.

347 The relationships between the joint opening and midspan deflection for specimens are plotted
348 in Fig. 14. It can be clearly seen from the figure that for all the specimens the joint showed an
349 almost linear relationship with the midspan deflection. Therefore, it can be stated that the width
350 of the vertical crack in case of the epoxied beam developed linearly with the midspan deflection
351 under the applied load. The joint opening was also plotted against the tendon stress in Fig. 15.
352 It is seen from the figures that in Beams BC1 and BC2, the stress in the CFRP tendons increased
353 approximately linearly with the joint opening up to ultimate stage. Meanwhile, Beam BS1
354 showed a non-linear relationship between the tendon stress and the joint opening. This
355 observation suggests the calculation of stress in the unbonded tendons of a segmental beam
356 based on the deflection of the beam by assuming the elongation of the tendon is equal to the
357 opening of the joint.

358 **4.2 Stress development in the tendon under applied load**

359 Fig. 16 shows the evolution of the prestressing tendon stress under four-point loading. The
360 corresponding envelop curves are plotted in Fig. 17. The effective stresses in the tendon at the

361 beginning of the loading process for beams BS1, BC1, and BC2 were 1280 MPa, 818 MPa and
362 661 MPa, respectively. It is seen from the figure that the tendon stress in all the beams started
363 to increase from the beginning of the test. The increase in the tendon stress was due to the
364 deflection of the beam under applied loads as such the applied load and tendon stress curves
365 are very similar to the curves of the applied load and deflection. From the figure, it can be seen
366 that the applied load vs tendon stress of the beams with CFRP tendons showed a bilinear
367 relationship but not for the beam with steel tendons. The one with steel tendon showed a highly
368 non-linear behaviour. It means the stress in the CFRP tendons increased nearly linearly to the
369 applied load, but with different increase rate before and after joint opening.

370 The tendon stress at the ultimate load in Beam BS1 was 1748 MPa, which was equal to 94%
371 of the nominal tensile strength of the prestressing steel tendons (1860 MPa). It is worth
372 mentioning that the test for Beam BS1 was stopped for the safety reason when large physical
373 damage was observed in the concrete on the top fibre (Fig. 8a). At that time, the prestressing
374 steel tendons already yielded but had not ruptured yet. After releasing the applied load, the
375 beam still recovered a certain deformation due to the retraction of steel tendons. In both Beams
376 BC1 and BC2, the CFRP tendons ruptured at the ultimate load. The tendon stresses at rupture
377 were 1774 MPa and 1687 MPa for Beams BC1 and BC2, respectively. It is worth noting that
378 these stress values were far below the nominal breaking strength of the CFRP tendon as they
379 were only equal to 72% and 69% of the breaking strength which was 2450 MPa as reported by
380 the manufacturer after carrying out 16 coupon tensile tests. This reduction in the tensile strength
381 of the CFRP tendons was affected by the loading type (bending loading), harping effect, and
382 the joint opening. Harped angle greatly prevents the increase in the tendon stress as shown in
383 previous studies [11-14]. In this study, a harping angle of 3° was used to avoid the strength
384 reduction exceeding 10% as recommended by Wang et al. [14]. Therefore, the joint opening
385 was responsible for low stress increment in CFRP tendons which requires further investigation.

386 After joint opening, the beams deformed at a much faster rate under the applied load so that
387 the increase in the tendon stress was much larger than that in the first stage when the beams
388 were still in the elastic region (Fig. 18). The total tendon stress increment in Beam BS1 was
389 468 MPa, which equals $0.25f_{pu}$ and those in Beams BC1 and BC2 were 956 MPa and 1026
390 MPa, which equal $0.33f_{pu}$ and $0.27f_{pu}$, respectively (Table 5).

391 **4.3 Tendon stress increment versus midspan deflection**

392 Fig. 19 shows the relationship between the tendon stress and vertical displacement of the
393 beams. It is seen from the curves that in all the beams, the tendon stress increment exhibited an
394 approximately linear relation to the midspan deflection up to the ultimate load regardless of the
395 type of tendons used. Even though, there was a slight variation in the curves of beams BS1 and
396 BC1 after joint opening. This observation is similar to previous studies conducted on
397 monolithic beams prestressed with unbonded tendons. Experimental tests by Tao and Du [30]
398 showed that there exists such linear relationship for moderately reinforced partially prestressed
399 concrete beams with unbonded steel tendons. Lou and Xiang [31] confirmed this observation
400 based on their numerical analysis. Wang et al. [14] also found this linear relationship between
401 tendon stress increment and midspan deflection when conducting tests on beams externally
402 prestressed with BFRP tendons. As such, this observation confirms the calculation procedure
403 for stress increment in the PSB prestressed with unbonded CFRP tendons based on midspan
404 deflection which have been used for monolithic beams [36, 37].

405 **4.4 Strain in rebars**

406 Since all the beams showed similar behaviour regarding the strain evolution in the ordinary
407 steel rebars under the applied loads, only the experimental results of Beam BS1 was given in
408 Fig. 20 for brevity, where R1 and R2 are the strains in the bottom and top longitudinal rebars;
409 R3, R4 and R5 and R6 are the strains in the stirrups of segment No.2 near middle joint J2, and

410 joint J3 as shown in Fig. 6, respectively. At the beginning, the strain in the top bars (R2) was
411 almost zero, while the bottom longitudinal bars were in compression with a strain of around -
412 300 $\mu\text{m}/\text{m}$ resulted from prestressing. When loads were applied, the top bars started to be
413 compressed, however, the strain developed in the bars at the ultimate stage was very small
414 since the strain gauge was attached in the middle of the segment which was far from the failure
415 position. Meanwhile, the stress in the bottom bars gradually changed from compression to
416 tension at cracking. The strain in the bottom bars was also very small at the ultimate load at
417 around 100 $\mu\text{m}/\text{m}$, which is far below the yielding point. This indicates that there is very small
418 contribution of longitudinal reinforcement bars to the loading capacity of segmental beams.
419 Yuan et al. [38] and Jiang et al. [39] reached the same conclusion in their studies on segmental
420 beams prestressed with steel tendons.

421 Steel stirrups near joint J2 developed a very small strain since J2 was in the pure bending region
422 under loading. The strain in the stirrups near J1 was also very small, even though J1 was in the
423 region with combined shear and bending. This indicates that the stirrups contributed little to
424 resisting the shear force at the joint locations as was also reported in the previous study [16].

425 **4.5 Residual displacement**

426 Fig. 21 shows the residual displacement at the end of each loading level of the specimens. It
427 can be seen from the figure that at the end of the load level just onset of the failure, the beams
428 prestressed with CFRP tendons underwent lesser residual displacement than the beam with
429 steel tendons. Beam BS1 underwent 8.06 mm residual displacement (0.22% L_b), while those
430 for Beams BC1 and BC2 were 5.47 mm (0.15% L_b) and 1.61 mm (0.04% L_b), respectively.
431 However, before opening of the joints, Beam BS1 had better performance than Beam BC1 as
432 it showed a smaller residual displacement after each load level. After joint opening, the residual
433 displacement sharply increased at the end of each load level in Beam BS1. Meanwhile, the

434 residual displacement in beam BC1 approximately increased linearly from the first to the last
435 loading level. As can be seen that replacing steel tendons by CFRP tendons resulted in a better
436 self-centring capacity of a PSB in which the beam could recover close to its original position
437 after excessive loading, for example from overloaded trucks.

438 Moreover, the epoxied joints greatly affect the behaviour of the beams with regards to the
439 residual deflection. It can be seen from the figure that beam BC2 underwent much lesser
440 residual deflection than Beam BC1. The experimental results have shown that the epoxied
441 joints can be used to achieve better self-centring capacity.

442 **5 Analytical calculations**

443 In this section, the accuracy of the current design procedures and equations recommended for
444 the calculation of the unbonded tendon stress at the ultimate load is evaluated. The examined
445 codes include AASHTO [18] , ACI 440.4R [4], ACI 318-14 [20] and BS 8110 [40]. However,
446 it is noted that except AASHTO [18], the equations for calculating tendon stress, f_{ps} ,
447 recommended by these codes are developed for the analysis of monolithic concrete beams, no
448 equation is provided in these codes to address segmental beams prestressed with unbonded
449 CFRP tendons. The design procedure presented in AASHTO [18] is used for segmental beams
450 prestressed with steel tendons. ACI 440.4R [4]'s equations are developed for monolithic beams
451 with CFRP tendons. ACI 318-14 [20] and BS 8110 [41] are for monolithic beams with steel
452 tendons. In brief, there is no specific design guide yet for segmental beams prestressed with
453 CFRP tendons.

454 For convenience, symbolic for the same parameter in different codes is modified to be identical.

455 AASHTO [18] adopted the following equation to predict the average stress in the unbonded
456 tendons in precast segmental concrete beams:

457
$$f_{ps} = f_{pe} + 6200 \left(\frac{d_{ps} - c}{l_e} \right), MPa \quad (2)$$

458 where f_{ps} is the effective tendon stress, d_{ps} is the distance from extreme top fibre to centroid of
 459 prestressing tendons, $l_e = L/(1+[N/2])$, in which L is the length of the tendon between
 460 anchorages, and N is the number of support hinges required to form a mechanism crossed by
 461 the tendon. The formula is based on the work of McGregor's research [35]. Up to date, there
 462 has been no recommendation by AASHTO [18] for FRP tendons in PSBs.

463 ACI 440.4R [4] recommended the following equation to predict the stress in CFRP tendons
 464 based on the work of Naaman et al. [41]:

465
$$f_{ps} = f_{pe} + \Omega_u E_{ps} \varepsilon_{cu} \left(\frac{d_{ps}}{c_u} - 1 \right) \quad (3)$$

466 where E_{ps} is the tendon modulus of elasticity; ε_{cu} is the ultimate concrete compression strain
 467 which was taken as 0.003; c_u is the neutral axis depth at ultimate loading; and Ω_u is a strain
 468 reduction coefficient defined as $\Omega_u = 1.5/(L_b/d_{ps})$ for one-point midspan loading and $\Omega_u =$
 469 $3/(L_b/d_{ps})$ for uniform or third-point loading, in which L_b is the span length. It is noted that Eq.
 470 3 was also used to calculate the stress in the unbonded steel tendons as it was originally
 471 developed for beams with steel tendons [4]. A limitation of $0.94 f_{py}$ was recommended in Eq.
 472 3 by Naaman and Alkhairi [27] based on the observation of experimental results, where f_{py} is
 473 the yield strength of steel tendons.

474 ACI 318-14 [20] suggested the following equation which is based on the research performed
 475 by Mattock et al. [42]:

476
$$f_{ps} = f_{pe} + 69 + \frac{f'_c}{100 \rho_{ps}}, MPa \quad (4)$$

477 where ρ_{ps} is the prestressing reinforcement ratio. This equation is applicable to beams with

478 $L/d_{ps} \leq 35$.

479 BS 8110 [41] recommended the following equation:

$$480 \quad f_{ps} = f_{pe} + \frac{7000}{d_{ps}} \left(1 - 1.7 \frac{f_{pu} A_{ps}}{f_{cu} b d_{ps}} \right), MPa \quad (5)$$

481 where A_{ps} is the area of prestressing tendons and f_{pu} is the nominal tensile stress at ultimate
482 loading of the tendon, b is the width of the cross-section, and f_{cu} is the cube strength of concrete
483 taken as $f'_{c}/0.8$.

484 The analytical and experimental results of the tendon stress and load capacity at ultimate
485 condition for all the specimens are listed in Table 5. The accuracy comparison of analytical
486 prediction of all code equations is shown in Fig. 22 and Fig. 23. As can be seen from Fig. 22,
487 all the code equations predicted well the ultimate stress for Beam BS1 with unbonded steel
488 tendons. It is worth mentioning that the result from Eq. 3 was taken as $0.94 f_{py}$ as recommend
489 by Naaman and Alkhairi [27] because the stress value from Eq. 3 was higher than $0.94 f_{py}$. This
490 value from Eq. 3 was, however, too conservative since in the test the steel tendons in Beam
491 BS1 already yielded. Results from AASHTO [18], ACI 318-14 [20], and BS 8110 [41]
492 equations are a bit larger than the experimental result for Beam BS1 since the test was stopped
493 for safety reason as mentioned previously.

494 The accuracy of the design equations in these codes considerably reduced in cases of the beams
495 with CFRP tendons as these codes are not specified for segmental beams with CFRP tendons.
496 AASHTO [18] and BS 8110 [41] equations underestimated f_{ps} by about 22% for Beam BC1
497 with dry joints and 28% for Beam BC2 with epoxied joint as compared with the experimental
498 results. ACI 318-14 [20] yielded the most conservative predictions at 31% and 36% lower than
499 the experimental results for Beams BC1 and BC2, respectively. Again, ACI 440.4R [4]'s
500 equation overestimated f_{ps} for both Beams BC1 and BC2 (Fig. 22). This is not common for a

501 code equation since a code normally yields conservative results. The reason for this substantial
502 difference may lie on the ratio L/d_{ps} . ACI 440.4R [4] limits the application of Eq. 3 for beams
503 with CFRP tendons having an unbonded length greater than 15 times the depth of the beam. In
504 this study, the ratio of unbonded tendon length to beam depth was equal to 9.

505 Similarly, except ACI 440.4R [4], all code equations predicted well P_u for beams with steel
506 tendons but less accurate when CFRP tendons were used. P_u predicted by AASHTO [18] and
507 BS 8110 [41] equations were respectively 18% and 16% lower than the experimental results
508 for the beams with dry joints, while those for the beams with epoxied joints were worse at 33%
509 and 31%, respectively. ACI 318-14 [20] underestimated P_u by 26% in the case of dry joint and
510 40% in the case of epoxied joints, respectively. ACI 440.4R [4] highly overestimated P_u due
511 to the fact that the L/d_{ps} used in this study was lower than the code's recommendation.

512 In order to verify the sensitivity of L/d_{ps} to the increase in the tendon stress of the tested beams
513 against the code equations, an analysis was made by plotting the tendon stresses computed by
514 the code equations against L/d_{ps} for all specimens. Only L/d_{ps} ratio was assumed to vary
515 between 7 and 45 while the other characteristics of the tested beams were kept constant. The
516 curves are shown in Fig. 24 for the case of beams with steel tendons and in Fig. 25 for beams
517 with CFRP tendons.

518 It can be seen from Fig. 24 that the change in the tendon stress is considerably influenced by the
519 ratio of L/d_{ps} in all codes, except ACI 318-14 [20] where the tendon stress at ultimate loading
520 only depends on f_{pe} , f'_c and ρ_{ps} as seen in Eq. 4. The increase in L/d_{ps} leads to the decrease in
521 the f_{ps} . As discussed previously, all codes predicted closely to the experimental results of Beam
522 BS1, except the prediction by Eq. 3. As such, the limitation of $0.94 f_{py}$ was used in the
523 calculation.

524 From Fig. 25, similar trend is observed between f_{ps} and L/d_{ps} for beams with CFRP tendons by

525 all codes. AASHTO [18], BS 8110 [41], and ACI 318-14 [20] underestimated the stress in the
526 tendon at ultimate condition. In which AASHTO [18] and BS 8110 [41] yielded similar
527 predictions, while ACI 318-14 [20] returned the least conservative result. ACI 440.4R [4]
528 overestimated f_{ps} at ultimate loading, however, both code prediction and experimental results
529 were far below the nominal breaking strength of the tendons. Therefore, the strain reduction
530 coefficient used by ACI 440.4R [4] in Eq. 3 is modified to $\Omega_u = 2.1 / (L/d_{ps})$ based on the
531 experimental results conducted in this study for segmental beams prestressed with CFRP
532 tendons. The curve of the modified Eq. 3 is also shown in Fig. 25.

533 **6 Conclusion**

534 An experimental study was conducted to evaluate the application of CFRP tendons on precast
535 segmental concrete beams. Three T-section segmental beams with either unbonded CFRP
536 tendons or steel tendons were built and tested under cyclic loads. Assessment of the four code
537 equations to predict the stress increment in the unbonded tendons was also presented. The main
538 findings are summarized as follows:

- 539 1. CFRP tendons can be well in replacement of steel tendons for segmental concrete beams.
540 They can assure the beams to achieve both good strength and ductility capacity.
- 541 2. The CFRP prestressed beam with dry joints performed similarly as the beam with unbonded
542 steel tendons in terms of overall load and deflection curve. They both showed non-linear load
543 and displacement relations after cracking. However, CFRP prestressed beams with epoxied
544 joints showed a linear load and displacement relation up to failure.
- 545 3. Unbonded CFRP tendons shifted the failure mode of under-reinforced beams from tension
546 controlled to compression controlled. This transition in the failure modes may prevent the
547 beams from a brittle failure manner when sudden rupture of the CFRP tendons in tension

548 occurs.

549 4. Epoxied or dry joints greatly affected the initial stiffness of the beams but had no effect on
550 the joint opening under the applied loads after cracking.

551 5. The average stress in the unbonded CFRP tendons for the beams with dry joints and epoxied
552 joints was only 72 % and 69% of the nominal tensile strength, respectively. The reduction in
553 the tendon stress at ultimate loading might be governed by the loading type, harping effect and
554 the joint opening which requires further investigation.

555 6. All the examined codes in this paper predicted well the unbonded steel tendon stress at
556 ultimate condition, however, the accuracy significantly reduced when CFRP tendons were
557 used. AASHTO [18] and BS 8110 [41] equations yielded better prediction among others, but
558 underestimated f_{ps} by approximately 22% for Beam BC1 with dry joints and 28% for Beam
559 BC2 with epoxied joint compared to the experimental results. A modification of ACI 440.4R
560 [4] code equation was suggested for segmental beams prestressed with unbonded CFRP
561 tendons to predict the stress in the tendon at ultimate loading.

562 7. Even though all the beams achieved similar deflection at the ultimate loading, the ductility
563 calculation showed large difference among these specimens. The reason might be due to the
564 sensitivity in determining the equivalent yielding point.

565 **7 Acknowledgements**

566 The authors would like to thank staff at the Civil Engineering laboratory, Curtin University,
567 especially Mr. Mick Elliss for their technical help during the experimental program. Thanks
568 are also expressed to Jaxier Koa and Xyrus Dangazo, final-year students for their great help in
569 the experimental works. Finally, the first author would like to acknowledge the Curtin Strategic
570 International Research Scholarship (CSIRS) and Centre for Infrastructural Monitoring and

571 Protection, School of Civil and Mechanical Engineering, Curtin University for the support of
572 his full PhD scholarship. The first author would also like to thank Hong Duc University, Thanh
573 Hoa, Vietnam for the support during his study course.

A_{ct}	area of the cross-section part between the flexural tension face and the centroid of the gross section
A_{ps}	area of prestressing tendons
A_u	area under the load-deflection curve at ultimate deflection
A_y	area under the load-deflection curve at yielding of tension steel
b	width of the cross-section
c	neutral axis depth of the section
c_u	neutral axis depth of the section at the ultimate condition
d	distance from the extreme top fibre to the centroid of tension force
d_{ps}	distance from extreme top fibre to centroid of prestressing tendons
f'_c	compressive concrete strength
f_{cu}	cube strength of concrete
f_{pe}	effective stress in the prestressing tendons after transfer
f_{pu}	ultimate tensile strength of prestressing tendons
f_{py}	yield strength of steel tendons
L	length of the tendon between anchorages
L_b	effective span length of the beam
N	number of support hinges
P_u	applied load at the ultimate loading condition
P_y	applied load at yielding
$\Delta_{J,u}$	opening of the middle joint at the ultimate loading condition
$\Delta_{J,y}$	opening of the middle joint at yielding
$\delta_{mid,u}$	midspan deflection at the ultimate loading condition
$\delta_{mid,y}$	midspan deflection at yielding
Δ_u	midspan deflection of the beam at the ultimate condition
Δ_y	midspan deflection of the beam at yielding of tension steel
ϵ_{cu}	ultimate compression strain of concrete
ϵ_{pe}	effective strain in the prestressing tendons
ϵ_{pu}	ultimate tensile strain of prestressing tendons
ρ_b, ρ_b^B	balanced reinforcement ratio of a beam with bonded tendons
ρ_b^U	balanced reinforcement ratio of a beam with unbonded tendons
ρ_{ps}	prestressing reinforcement ratio
ω_{ps}	reinforcement index
Ω_u	strain reduction coefficient

577 **8 References**

- 578 [1] Woodward R, Williams F. Collapse of YNS-Y-GWAS Bridge, Glamorgan. *Proc Inst Civ*
579 *Eng* 1988;84(4):635-69.
- 580 [2] Wouters J, Kesner K, Poston R. Tendon corrosion in precast segmental bridges. *Transp Res*
581 *Rec J Transp Res Board* 1999(1654):128-32.
- 582 [3] Concrete Society Technical Report. Durable post-tensioned concrete structures. TR 72,
583 2002.
- 584 [4] ACI 440.4R. Prestressing concrete structures with FRP tendons. Farmington Hills, USA:
585 American Concrete Institute; 2004.
- 586 [5] Dolan CW, Swanson D. Development of flexural capacity of a FRP prestressed beam with
587 vertically distributed tendons. *Compos B Eng* 2002;33(1):1-6.
- 588 [6] Maissen A, de Smet CA. Prestressed concrete using carbon fibre reinforced plastic (CFRP)
589 strands. *Mater Struct* 1998;31(3):175-7.
- 590 [7] Zou PXW. Flexural Behavior and Deformability of Fiber Reinforced Polymer Prestressed
591 Concrete Beams. *J Compos Constr* 2003;7(4):275-84.
- 592 [8] Lou T, Lopes SMR, Lopes AV. Numerical analysis of behaviour of concrete beams with
593 external FRP tendons. *Constr Build Mater* 2012;35:970-8.
- 594 [9] Tan KH, Tjandra RA. Strengthening of RC continuous beams by external prestressing. *J*
595 *Struct Eng* 2007;133(2):195-204.
- 596 [10] Pisani MA. A numerical survey on the behaviour of beams pre-stressed with FRP cables.
597 *Constr Build Mater* 1998;12(4):221-32.
- 598 [11] Mutsuyoshi H, Machida A. Behavior of Prestressed Concrete Beams Using FRP as
599 External Cable. *Spec Publ* 1993;138:401-18.
- 600 [12] Grace NF, Abdel-Sayed G. Behavior of externally draped CFRP tendons in prestressed
601 concrete bridges. *PCI J* 1998;43(5):88-101.
- 602 [13] Quayle TG. Tensile-flexural Behaviour of Carbon-fibre Reinforced Polymer (CFRP)
603 Prestressing Tendons Subjected to Harped Profiles: MS thesis. Univ. Waterloo; 2005.
- 604 [14] Wang X, Shi J, Wu G, Yang L, Wu Z. Effectiveness of basalt FRP tendons for
605 strengthening of RC beams through the external prestressing technique. *Eng Struct*
606 2015;101:34-44.
- 607 [15] Jiang H, Chen L, Ma ZJ, Feng W. Shear Behavior of Dry Joints with Castellated Keys in
608 Precast Concrete Segmental Bridges. *J Bridge Eng* 2015;20(2):04014062.
- 609 [16] Li G, Yang D, Lei Y. Combined shear and bending behavior of joints in precast concrete
610 segmental beams with external tendons. *J Bridge Eng* 2013;18(10):1042-52.
- 611 [17] Turmo J, Ramos G, Aparicio AC. Shear strength of dry joints of concrete panels with and
612 without steel fibres. Application to precast segmental bridges. *Eng Struct* 2006;28(1):23-33.
- 613 [18] AASHTO. Guide Specifications for Design and Construction of Segmental Concrete
614 Bridges, 2nd Ed with 2003 Interim Revis. Washington, DC: American Association of State
615 Highway and Transportation Officials; 1999.
- 616 [19] Zhou X, Mickleborough N, Li Z. Shear strength of joints in precast concrete segmental
617 bridges. *ACI Struct J* 2005;102(1):3.
- 618 [20] ACI 318-14. Building code requirements for structural concrete and commentary:
619 American Concrete Institute. International Organization for Standardization; 2015.
- 620 [21] AS 1012.8.1. Methods of testing concrete - Method 8.1: Method for making and curing
621 concrete—Compression and indirect tensile test specimens. Standards Australia International

622 Ltd, NSW 2014.

623 [22] AS 1012.9. Methods of testing concrete - Method 9: Compressive strength tests—
624 Concrete, mortar and grout specimens. Standards Australia International Ltd, NSW 2014.

625 [23] Dextra Group. CFRP tendons. [https://www.dextragroup.com/offices/dextra-building-](https://www.dextragroup.com/offices/dextra-building-products-limited)
626 [products-limited.](https://www.dextragroup.com/offices/dextra-building-products-limited)

627 [24] Sika Australia. Sikadur-30. [https://aussikacom/.](https://aussikacom/)

628 [25] Bestech Company. [https://www.bestech.com.au/.](https://www.bestech.com.au/)

629 [26] AASHTO LRFD. Bridge Construction Specifications, 6th Edition, U.S. Units.
630 Washington, DC: American Association of State Highway and Transportation Officials; 2012.

631 [27] Naaman AE, Alkhairi F. Stress at ultimate in unbonded prestressing tendons: Part 2—
632 Proposed Methodology. *ACI Struct J* 1991;88(6):683-92.

633 [28] Lee C, Shin S, Lee H. Balanced Ratio of Concrete Beams Internally Prestressed with
634 Unbonded CFRP Tendons. *Int J Concr Struct Mater* 2017;11(1):1-16.

635 [29] Saibabu S, Srinivas V, Sasmal S, Lakshmanan N, Iyer NR. Performance evaluation of dry
636 and epoxy jointed segmental prestressed box girders under monotonic and cyclic loading.
637 *Constr Build Mater* 2013;38:931-40.

638 [30] Tao X, Du G. Ultimate stress of unbonded tendons in partially prestressed concrete beams.
639 *PCI J* 1985;30(6):72-91.

640 [31] Lou T, Xiang Y. Effects of ordinary tension reinforcement on the response of beams with
641 unbonded tendons. *Adv Struct Eng* 2007;10(1):95-109.

642 [32] Park R. Evaluation of ductility of structures and structural assemblages from laboratory
643 testing. *Bull N Z Natl Soc Earthq Eng* 1989;22(3):155-66.

644 [33] Harajli MH. On the stress in unbonded tendons at ultimate: Critical assessment and
645 proposed changes. *ACI Struct J* 2006;103(6):803.

646 [34] Lee L-H, Moon J-H, Lim J-H. Proposed methodology for computing of unbonded tendon
647 stress at flexural failure. *Struct J* 1999;96(6):1040-8.

648 [35] Roberts-Wollmann CL, Kreger ME, Rogowsky DM, Breen JE. Stresses in external
649 tendons at ultimate. *ACI Struct J* 2005;102(2):206.

650 [36] He Z, Liu Z. Stresses in External and Internal Unbonded Tendons: Unified Methodology
651 and Design Equations. *J Struct Eng* 2010;136(9):1055-65.

652 [37] Harajli M, Kanj M. Ultimate flexural strength of concrete members prestressed with
653 unbonded tendons. *Struct J* 1992;88(6):663-74.

654 [38] Yuan A, Dai H, Sun D, Cai J. Behaviors of segmental concrete box beams with internal
655 tendons and external tendons under bending. *Eng Struct* 2013;48:623-34.

656 [39] Jiang H, Cao Q, Liu A, Wang T, Qiu Y. Flexural behavior of precast concrete segmental
657 beams with hybrid tendons and dry joints. *Constr Build Mater* 2016;110:1-7.

658 [40] BS 8110. Structural use of concrete. London: British Standards Institution; 1997.

659 [41] Naaman AE, Burns N, French C, Gamble WL, Mattock AH. Stresses in unbonded
660 prestressing tendons at ultimate: Recommendation. *Struct J* 2002;99(4):518-29.

661 [42] Mattock AH, Yamazaki J, Kattula BT. Comparative study of prestressed concrete beams,
662 with and without bond. *J Proc* 1971;68(2):116-25.

663

664 **9 List of Figures**

665 Fig. 1. Detailed dimensions of tested beams

666 Fig. 2. Multiple shear-keyed joints

667 Fig. 3: Casting of specimens

668 Fig. 4: Typical set up for post-tensioning

669 Fig. 5: CFRP tendon with steel couplers

670 Fig. 6: Typical test set up

671 Fig. 7: Progressive loading cycles

672 Fig. 8: Failure modes of the tested specimens

673 Fig. 9: Load vs deflection curves

674 Fig. 10: Envelop curves of load vs deflection

675 Fig. 11: Definition of yielding point

676 Fig. 12: Opening of joints along beam's axis

677 Fig. 13: Applied load vs opening of middle joint J2 of specimens

678 Fig. 14: Relationship between joint opening vs midspan deflection

679 Fig. 15: Tendon stress vs joint opening

680 Fig. 16: Applied load vs tendon stress of specimens

681 Fig. 17: Envelop curves of applied load vs tendon stress

682 Fig. 18: Envelop curves of applied load vs tendon stress increment

683 Fig. 19: Tendon stress vs midspan deflection

- 684 Fig. 20: Strain in rebars in Beam BS1
- 685 Fig. 21: Residual displacement of specimens
- 686 Fig. 22: Comparison of calculation of f_{ps}
- 687 Fig. 23: Comparison of calculation of P_u
- 688 Fig. 24: Relationship between f_{ps} and L/d_{ps} ratio for beams with steel tendons
- 689 Fig. 25: Relationship between f_{ps} and L/d_{ps} ratio for beams with CFRP tendons

690 **10 List of Tables**

691 Table 1: Configuration of tested beams

692 Table 2: Properties of materials

693 Table 3: Experimental testing results

694 Table 4: Ductility of the specimens

695 Table 5: Theoretical calculation of the four codes

List of Figures

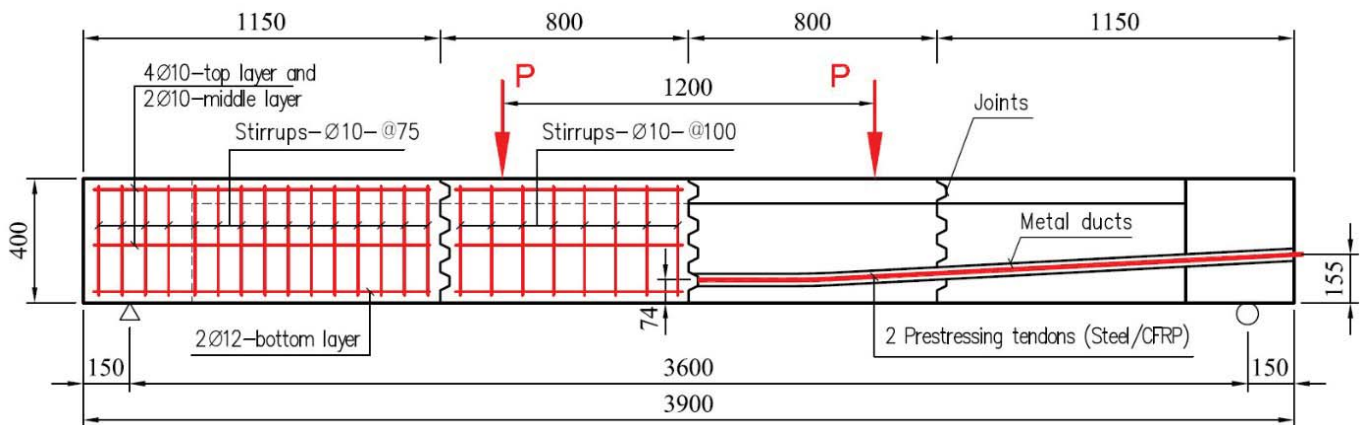


Fig. 1. Detailed dimensions of tested beams

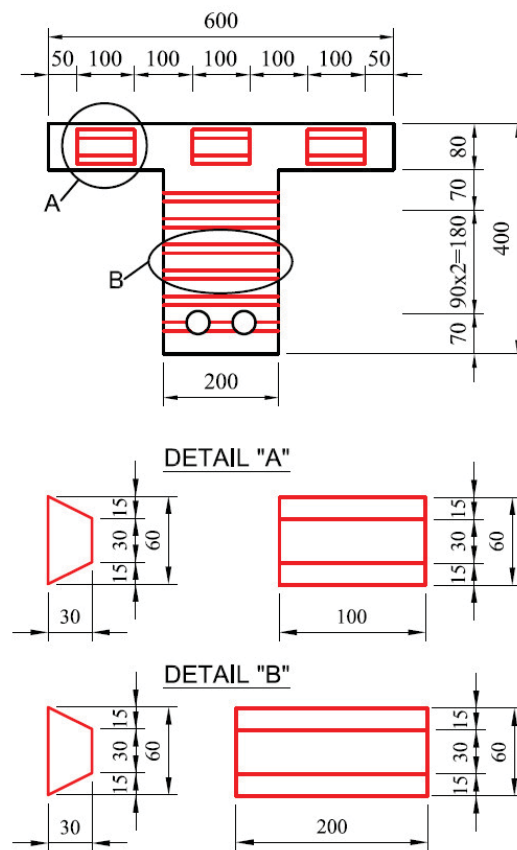


Fig. 2. Multiple shear-keyed joints



Fig. 3: Casting of specimens

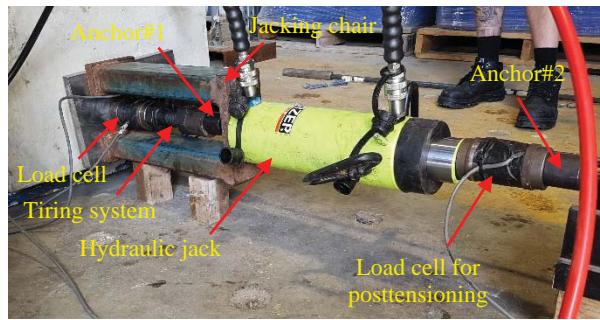


Fig. 4: Typical set up for post-tensioning

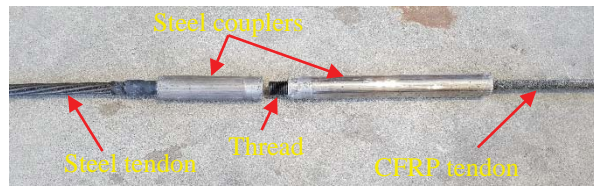


Fig. 5: CFRP tendon with steel couplers

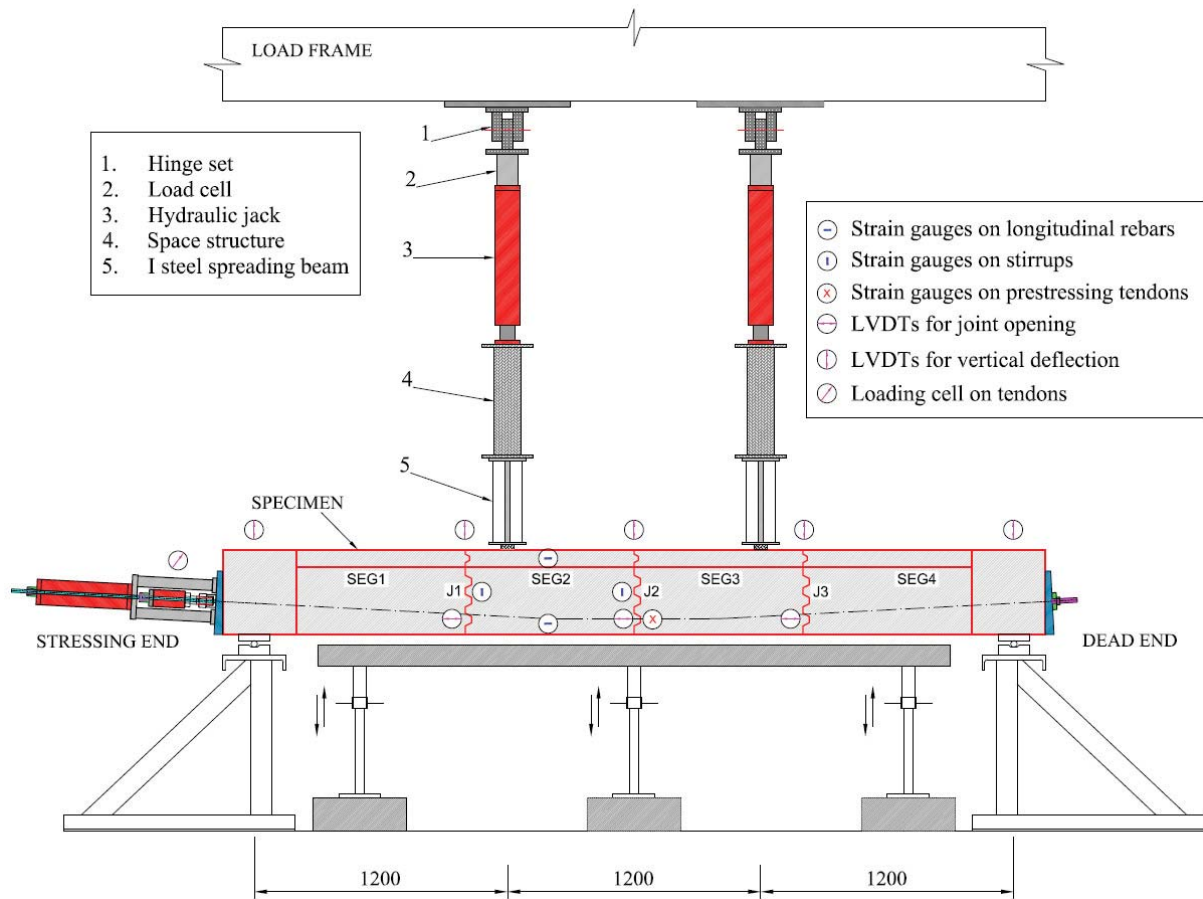


Fig. 6: Typical test set up

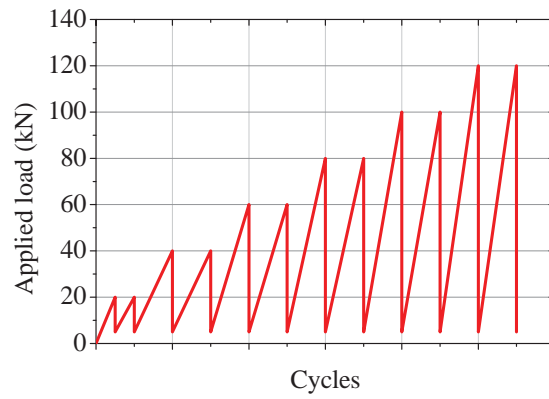


Fig. 7: Progressive loading cycles

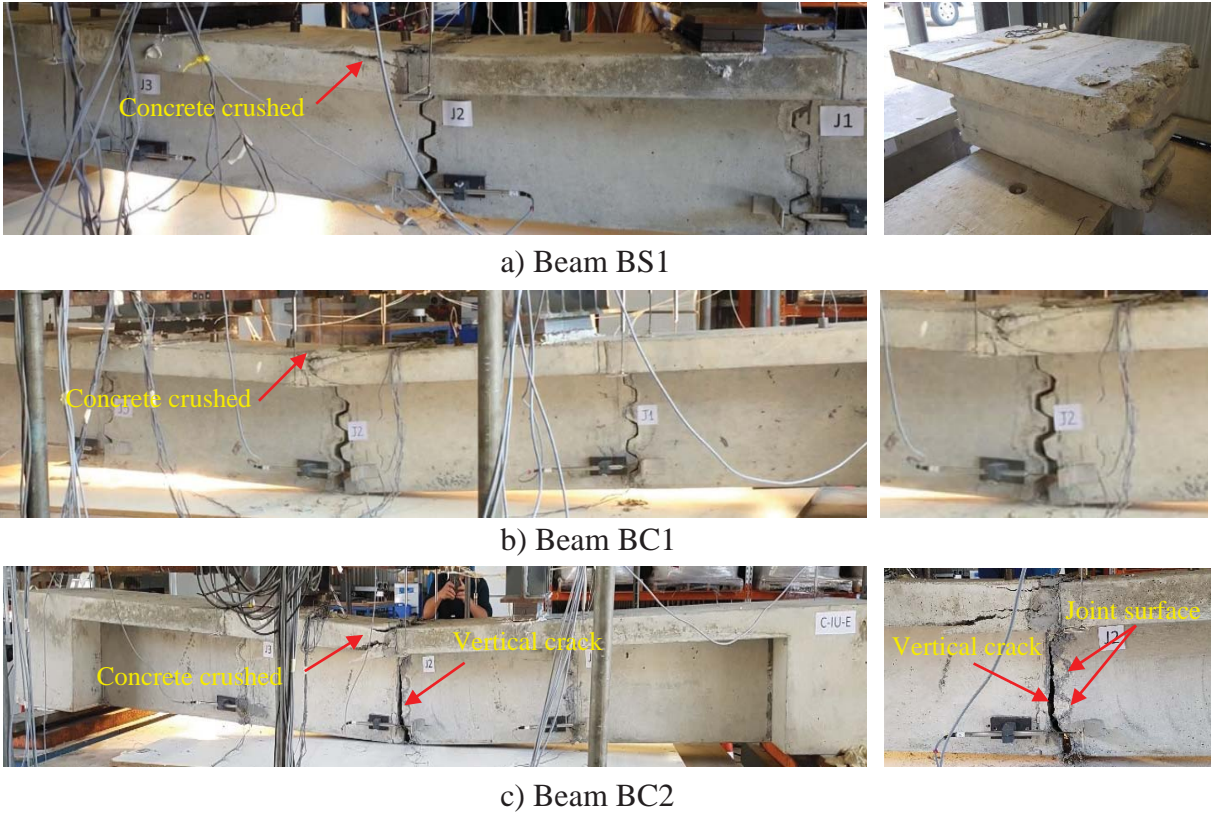


Fig. 8: Failure modes of the tested specimens

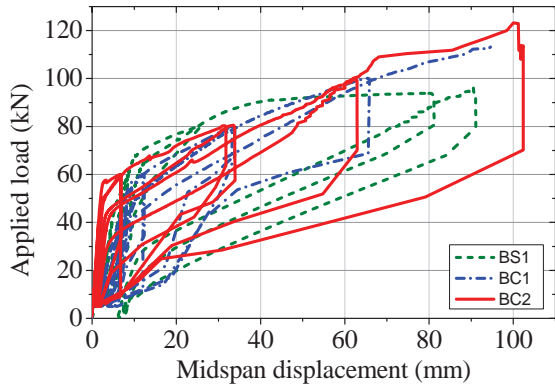


Fig. 9: Load vs deflection curves

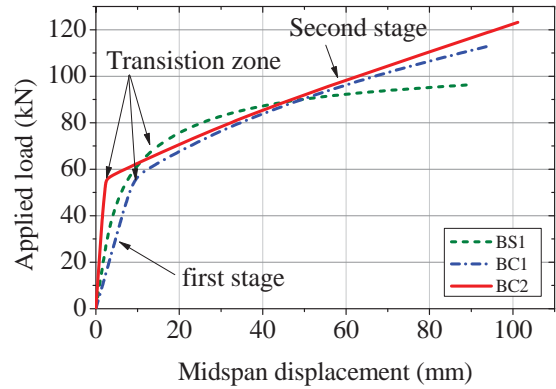


Fig. 10: Envelop curves of load vs deflection

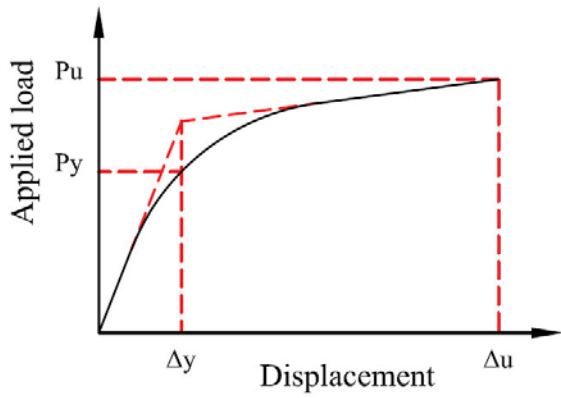


Fig. 11: Definition of yielding point

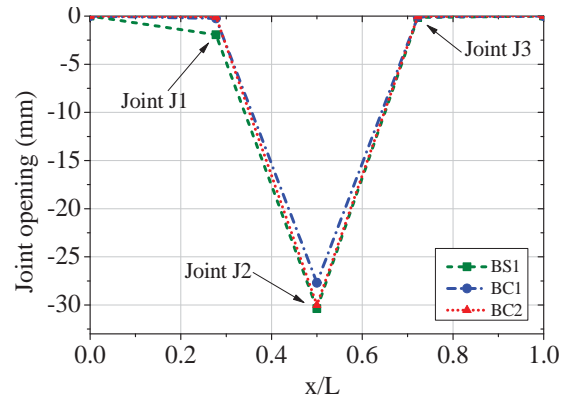


Fig. 12: Opening of joints along beam's axis

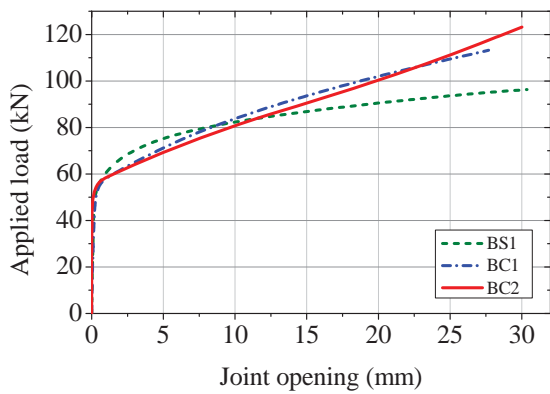


Fig. 13: Applied load vs opening of middle joint J2

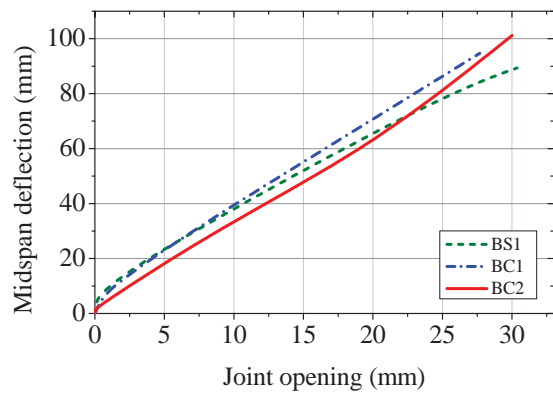


Fig. 14: Relationship between joint opening vs midspan deflection

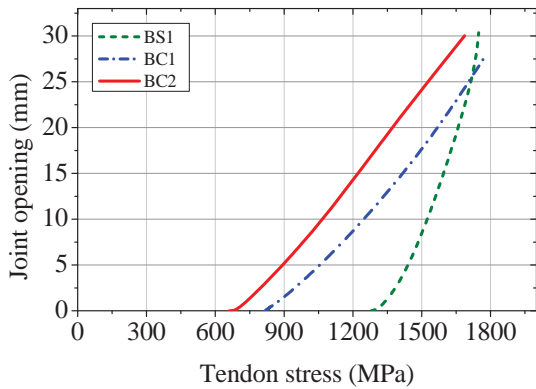


Fig. 15: Tendon stress vs joint opening

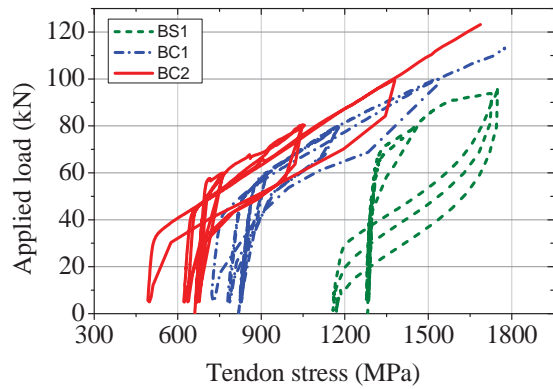


Fig. 16: Applied load vs tendon stress

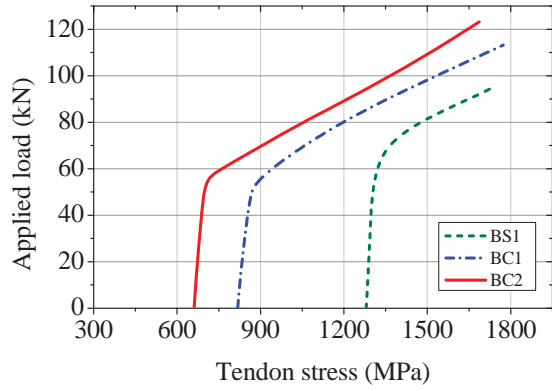


Fig. 17: Envelop curves of applied load vs tendon stress

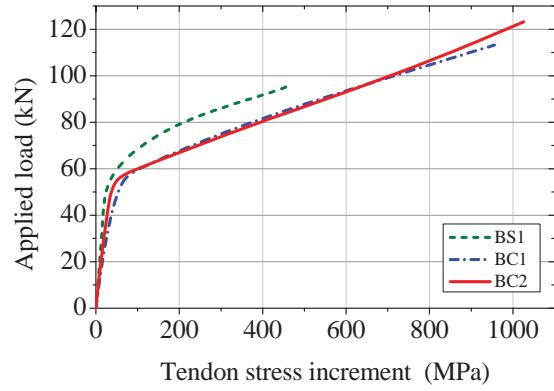


Fig. 18: Envelop curves of applied load vs tendon stress increment

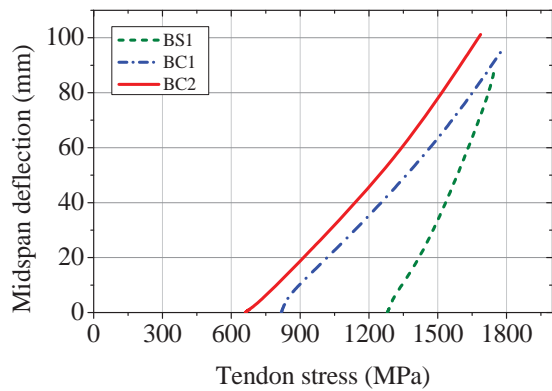


Fig. 19: Tendon stress vs midspan deflection

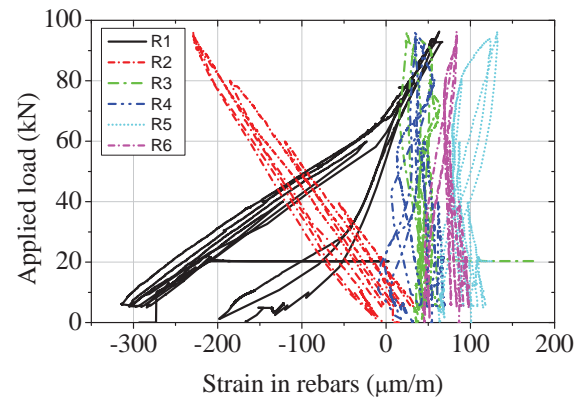


Fig. 20: Strain in rebars in Beam BS1

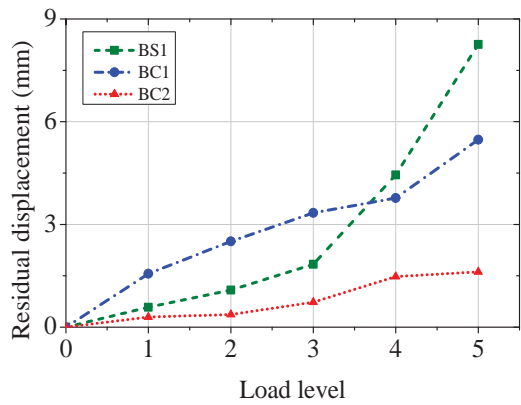


Fig. 21: Residual displacement of specimens

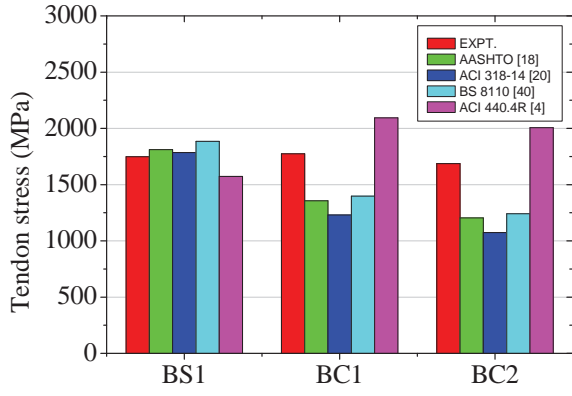


Fig. 22: Comparison of calculation of f_{ps}

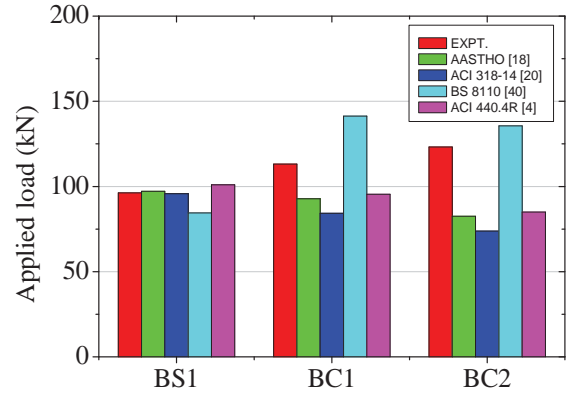


Fig. 23: Comparison of calculation of P_u

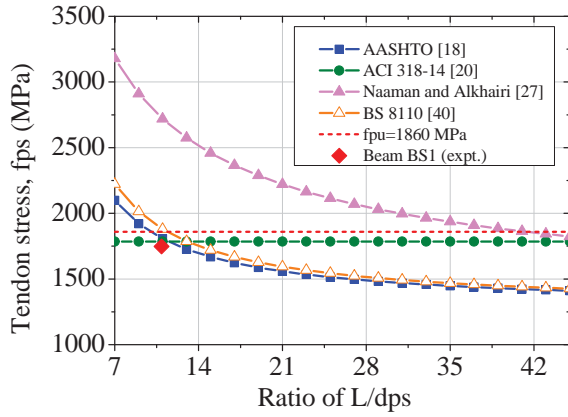


Fig. 24: Relationship between f_{ps} and L/d_{ps} ratio for beams with steel tendons

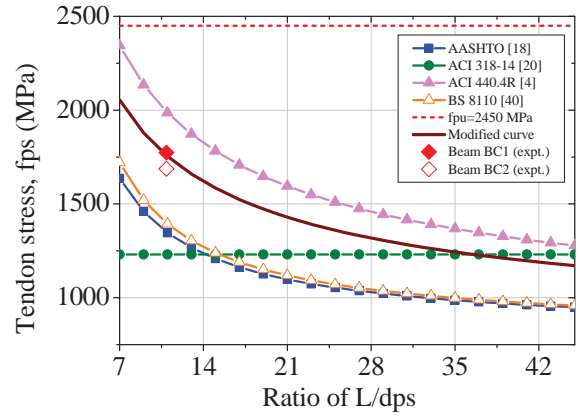


Fig. 25: Relationship between f_{ps} and L/d_{ps} ratio for beams with CFRP tendons

List of Tables

Table 1: Configuration of tested beams

Specimen	Tendon type	Joint type	Concrete strength	Effective tendon stress		Tendon force
			f_c' (MPa)	f_{pe} (MPa)	f_{pe}/f_{pu}	F_{pe} (kN)
BS1	2 steel tendons	Dry	44	1193	0.64	119
BC1	2 CFRP tendons	Dry	44	851	0.35	108
BC2	2 CFRP tendons	Epoxied	44	653	0.27	83

Table 2: Properties of materials

Type	Diameter (mm)	Area (mm ²)	Yield strength (MPa)	Ultimate strength (MPa)	Elastic modulus (GPa)
12-mm steel bars N12	12.0	113.0	534	587	200
10-mm steel bars N10	10.0	78.5	489	538	200
Steel tendon	12.7	100.0	1674	1860	195
CFRP tendon	12.9	126.7	N/A	2450	145

Table 3: Experimental testing results

Specimen	Applied load (kN)		Midspan deflection (mm)		Joint opening (mm)		Failure mode
	P_y	P_u	$\delta_{mid,y}$	$\delta_{mid,u}$	$\Delta_{J,y}$	$\Delta_{J,u}$	
BS1	51.2	96	5.4	89.4	0.20	30.44	Compression failure and yielding of tendons
BC1	53.4	113	8.4	94.7	0.55	27.70	Compression failure and rupture of CFRP tendons
BC2	54.1	123	2.3	101.1	0.07	30.02	Compression failure and rupture of CFRP tendons

Table 4: Ductility of the specimens

Specimen	Method 1			Method 2		
	Δ_y	Δ_u	Δ_u/Δ_y	A_y	A_u	A_u/A_y
BS1	5.4	89.4	16.6	201	7298	36.3
BC1	8.4	94.7	11.2	336	7853	23.4
BC2	2.3	101.1	44.0	67	9154	136.6

Table 5: Theoretical calculation of the four codes

Specimen	f_{pe} (MPa)	Δf_{ps} (MPa)			f_{ps} (MPa)			P_u (kN)				
		Theo.	Expt.	Theo/Expt	Theo.	Expt.	Theo/Expt	fexpt/fu	Theo.	Expt.	Theo/Expt	
AASHTO [18]												
BS1	1280	531	468	1.13	1811	1748	1.04	0.94	97	96	1.01	
BC1	818	539	956	0.56	1357	1774	0.76	0.72	93	113	0.82	
BC2	661	543	1026	0.53	1204	1687	0.71	0.69	83	123	0.67	
ACI 318-14 [20]												
BS1	1280	505	468	1.08	1785	1748	1.02	0.94	96	96	0.99	
BC1	818	413	956	0.43	1231	1774	0.69	0.72	84	113	0.74	
BC2	661	413	1026	0.40	1074	1687	0.64	0.69	74	123	0.60	
ACI 440.4R [4]												
BS1	1280	294	468	0.63	1574	1748	0.90	0.94	84	96	0.88	
BC1	818	1276	956	1.33	2094	1774	1.18	0.72	141	113	1.25	
BC2	661	1345	1026	1.31	2006	1687	1.19	0.69	136	123	1.10	
BS 8110 [40]												
BS1	1280	604	468	1.29	1884	1748	1.08	0.94	101	96	1.05	
BC1	818	579	956	0.61	1397	1774	0.79	0.72	95	113	0.84	
BC2	661	579	1026	0.56	1241	1687	0.74	0.69	85	123	0.69	